Flow interactions with an aquatic macrophyte: a field study using stereoscopic particle image velocimetry

Flow interactions with an aquatic macrophyte: a field study using stereoscopic Particle Image Velocimetry (PIV)

H. J. Biggs[a*], V. I. Nikora[b], C. N. Gibbins[c], S. M. Cameron[b], K. Papadopoulos[b], M. Stewart[b], S. Fraser[d], D. Vettori[e], M. Savio[b], M. T. O'Hare[f], M. Kucher[g] and D. M. Hicks[a]

[a]Sediment Processes Group, National Institute of Water and Atmospheric Research (NIWA), Christchurch, New Zealand; [b]School of Engineering, University of Aberdeen, Aberdeen, UK; [c]School of Environmental and Geographical Sciences, University of Nottingham Malaysia Campus, Selangor Darul Ehsan, Malaysia; [d]NAFC Marine Centre, University of the Highlands and Islands, Scalloway, Shetland, UK; [e]Department of Geography and Environment, Loughborough University, Loughborough, UK; [f]Centre for Ecology & Hydrology (CEH), Edinburgh, UK; [g]Institute of Lightweight Engineering and Polymer Technology, Technische Universität Dresden, Dresden, Germany.

*Contact: Hamish.Biggs@niwa.co.nz

Flow interactions with an aquatic macrophyte: a field study using stereoscopic Particle Image Velocimetry (PIV)

This paper reports the morphology of a natural patch of *Ranunculus penicillatus* and presents high-resolution measurements of flow velocities in its wake using a stereoscopic PIV field measurement system. The patch was 3.80 m long, 1.24 m wide and caused substantial changes to downstream mean velocities and turbulence. Vertical profiles of streamwise mean velocity were not logarithmic and flow was redirected under the positively buoyant canopy, enhancing vertical turbulent mixing in the wake and generating a large region where the velocity covariance $\overline{u'w'}$ was positive. Turbulent kinetic energy was enhanced downstream from the patch lateral shear layer, but not at the centre of the wake. Spectra downstream from the patch showed that turbulence was neither dominated by fine-scale nor large-scale structures, likely due to the low energy of the flow conditions and lack of a developed vortex street within the measurement domain. Sedimentation was observed at the upstream end of the patch, but not underneath the floating canopy. The methods and results of this work will be useful for planning other in situ studies. Also, the reported data on macrophyte geometry and biometrics will assist with the design of more realistic replicas for use in laboratory studies.

Keywords: Aquatic vegetation; macrophyte; PIV; turbulence; wake; sediment; flow-vegetation interactions; vegetation management; ecohydraulics.

1. Introduction

Aquatic macrophytes are prevalent in lowland rivers globally. They are a porous obstruction that provides habitat for invertebrates and fish (Shupryt & Stelzer, 2009; Figueiredo *et al*., 2015). Macrophytes affect river hydraulics by increasing flow resistance, which decreases river velocities, increases depths and enhances deposition of suspended sediment (Butcher, 1933). Reduced suspended sediment improves the optical clarity of water for instream organisms, but causes a feedback loop of vegetation proliferation as light transmission improves (Madsen *et al*., 2001). At high macrophyte biomass river conveyance is negatively affected, resulting in river management problems such as excessive sedimentation and increased flood risk (Butcher, 1933; Gurnell *et al*., 2006). To avoid these negative effects, aquatic vegetation may be mechanically removed

from rivers, usually at significant cost (Bal & Meire, 2009; Dawson, 1989). However, mechanical removal of aquatic vegetation can cause a dramatic increase in suspended sediment (Greer *et al*., 2017) with negative ecological consequences for invertebrates and fish (Garner *et al*., 1996; Kemp *et al*., 2011). Improved management strategies are needed to balance river ecology with practical engineering considerations. These strategies should be based on accurate quantification of macrophyte abundance (Biggs *et al*., 2018), coupled with rigorous understanding of the effect of macrophytes on flow characteristics and river morphology.

Macrophytes interact with flow across a range of spatial scales (Nikora, 2010; Nepf, 2012). At the sub-leaf scale, nutrient flux is a function of leaf boundary layer thickness and flow-leaf interactions (Nishihara & Ackerman, 2006; Nepf, 2012). At the leaf/stem scale, drag forces and reconfiguration are a function of plant morphology, mean flow velocities and turbulence (Albayrak *et al*., 2012; 2014). At the plant/patch scale, macrophyte biomechanics and upstream turbulence influence morphology and drag forces (Siniscalchi & Nikora, 2012; 2013). The estimation of total drag force based on morphology is challenging, as total patch drag is not a simple summation of the drag forces on individual stems and leaves (Albayrak *et al*., 2014). At the river reach scale, drag forces and turbulence are dependent on the geometry, density and spacing of macrophyte patches (Folkard, 2011). Large scale turbulence in patch wakes and the formation of wake eddies is a function of patch porosity (Chang & Constantinescu, 2015; Taddei *et al.*, 2016), with porous patches delaying vortex street formation (Zong & Nepf, 2012). Kelvin-Helmholtz vortices can also form in the lateral shear layer of vegetation patches and may influence mixing within macrophyte canopies (Rominger & Nepf, 2011). Vegetation drag at the patch mosaic scale can also modify river hydraulic

conditions, with implications for sediment transport processes, river morphology and flooding (Gurnell *et al*., 2006; Gurnell, 2014).

To investigate flow-vegetation interactions in controlled conditions (e.g. laboratory flumes), it is common to use geometric analogues such as rigid cylinder arrays or flexible replica vegetation. Rigid cylinder arrays have been used extensively and provide a good geometric analogue for rigid elements such as mangrove roots, or reedy emergent vegetation. However, they are a poor surrogate for flexible submerged vegetation (Abdolahpour *et al*., 2018; Boothroyd *et al*., 2016). Other replica vegetation such as cylinders with plastic flexible leaves attached (Abdolahpour *et al*., 2018; Hu *et al*., 2018) provide a plausible analogue for plants with simple morphologies, but it is not well established whether this approach could be employed to represent natural macrophytes in rivers. An alternative approach to using replica vegetation for studies of flow-macrophyte interactions is to use reduced scale macrophyte patch surrogates that are constructed of real macrophyte stems (Siniscalchi *et al*., 2010). However, it is challenging to upscale these results, as larger scale processes (such as patch drag forces) are not the result of a simple summation of processes at smaller scales because of the effects of clumping and reconfiguration (Albayrak *et al*., 2014).

A promising method for investigating flow interactions with aquatic macrophytes is to study natural patches *in situ* using high resolution particle image velocimetry. This approach was successfully employed by Cameron *et al*., (2013) who used stereoscopic PIV to study a small patch of *Ranuculus penicillatus* (length = 0.4 m) in the River Urie in North East Scotland. PIV measurements resolve the motion of neutrally buoyant tracer particles as they move with fluid flow (Raffel *et al*., 2007). They are well suited to

investigate flows with high spatial and temporal heterogeneity (Stamhuis, 2006), such as the wake of aquatic macrophytes. The current study continues the approach of studying macrophytes *in situ* in Scottish rivers, but uses an upgraded field stereoscopic PIV system compared to that of Nikora *et al*., (2012) and Cameron *et al*., (2013). The system upgrades enabled high-resolution flow measurements around much larger *R. penicillatus* patches (over 3 m long), which are representative of specimens commonly found in the UK at the end of the summer growing season (Biggs *et al*., 2018). The objectives of this study were to evaluate the geometry and biometric characteristics of *R. penicillatus* patches (1) and the *in situ* flow characteristics downstream from a patch, covering: (2) mean flow velocities; (3) turbulent kinetic energy; (4) velocity covariances and their spatial gradients; (5) velocity spectra and skewness; and (6) sedimentation.

2. Materials and methods

2.1. Study reach and background conditions

The study took place on the 13th of August 2015 in a 100 m reach of the Luther Water in North East Scotland (Figure 1). The study reach was approximately 5 m wide, was vegetated with *R. penicillatus* patches and had a water surface slope of 0.00334. Water surface slope was measured with a piezometric system that consisted of two pressure receivers separated by a tube 100 m long. This allowed measurements of water surface slope with a base of 100 m. The studied *R. penicillatus* patch was 3.80 m long, 1.24 m wide and was in a section of the reach that was relatively free from other vegetation. Background hydraulic conditions in the reach were considered nearly steady during PIV measurements, with a 2% change in discharge and 3-4 mm reduction in water surface level (compared to an average water depth of 350-400 mm). The bed was predominantly

formed of stones/cobbles, with sand and silt accumulating between them. Upstream from the measurement planes the maximum cobble size was 125 mm, while the median was 46 mm (n = 100). The Luther Water measurement site is situated near the town of Laurencekirk and drains a catchment of ~100 km^2 which is comprised of a mixture of agricultural, forested hillslopes and mountainous terrain.

2.2. Field stereoscopic PIV system and set-up

The field stereoscopic PIV system used in this study (Figure 2) is a comprehensively upgraded version of that described by Nikora *et al*., (2012) and Cameron *et al*., (2013). Its key components are: (1) an aluminium bridge structure (dimensions 4 m by 9 m) with adjustment possibility in all three spatial directions and 16.25 m^2 effective river interrogation area; (2) an Oxford Lasers Nano-L-50/100 PIV, 100 mJ twin Nd:YAG laser with two laser power supplies; (3) four Dalsa 4M60 global shutter cameras with Nikon 60 mm lenses, Scheimpflug adapters and 532 nm bandpass optical filters; (4) two computers with frame grabbers and 16 direct-to-disk hard drives; (5) a glass bottom 'boat'; (6) a constant head seeding distribution system; and (7) a 6.5 kW SDMO Kohler Technic generator.

Deployment of the PIV system was a complex operation. First, the study reach topography was surveyed from the air and ground (Biggs *et al*., 2018), with river banks then levelled for installation of the X axis of the PIV bridge structure (Figure 2). The PIV system hardware was assembled in a laboratory and calibrated in a large tank prior to transporting it to the field. The field installation, data recording and disassembly took 15 hours (from dawn to dusk), with a team of 10 scientists and technicians. Following field deployment, calibrations were re-checked in the laboratory to ensure that the alignment

of the rigidly fixed components (cameras, glass bottom boat and laser optics) had not changed during transportation.

Conifer pollen was used as seeding/tracer in the study because it is biodegradable, has particle diameter of 60-80 microns and is almost neutrally buoyant (Cameron *et al*., 2013). Seeding particles were added to the river water at approximately 100g/minute, from 3-4 locations upstream from the patch. The PIV settings were: laser frequency of 32 Hz per laser; 1 ms delay between laser pulses; cameras recording images at 64 Hz; camera interrogation area of 2352×1528 pixels; and a 2 mm output grid for velocity vectors. Velocity vectors are derived from image pairs and are output at a frequency of 32 Hz. The PIV system was deployed in a cross-stream orientation, with each measurement plane being 10 cm wide and extending from the bed to the water surface.

2.3. PIV measurements

PIV measurements (Figure 3) consisted of 28 PIV planes with 10 minutes duration per plane and provided over 1.2×10^{10} velocity vectors in total. To assess the effects of the *R. penicillatus* patch on the flow, PIV measurements were taken in three vegetation configurations: (1) the natural patch *in situ* (Figure 4a); (2) the patch trimmed to approximately 20% of its initial biomass (Figure 4b); and (3) the patch completely removed to provide a rough bed (free of vegetation) control. Most measurements were performed in the wake of the natural patch, with planes P01 to P12 in the near wake (0.5 m downstream from the patch end) and planes P13 to P24 in the far wake (2.31 m downstream from the patch end) (Figure 3, Figure 5). After the patch was trimmed two planes were repeated in the near wake ($P01_T$ and $P06_T$). After the patch was removed the same planes were repeated as a rough bed control ($P01_R$ and $P06_R$). A right-handed coordinate system (Figure 3, Figure 5) was used to provide consistency with other studies

of flow vegetation interactions (e.g. Nepf, 2012; Cameron *et al*., 2013; Chang & Constantinescu, 2015; Boothroyd *et al*., 2017).

2.4. PIV data processing and analysis

PIV data processing and system calibration was performed as per Cameron (2011), Cameron *et al.*, (2013), and Stewart (2014) using the *Slugflow* software package developed in-house by Dr S. Cameron. Iterative Deformation Method (IDM) analysis algorithms were used, with 96x96 pixel interrogation regions and 8 analysis passes. After the image data were processed, flow velocity vectors were output for post-processing, with the calculation of hydraulic parameters being performed in *Slugflow* and *Matlab*.

The motion of water in rivers is generally described by the Navier-Stokes equations for instantaneous variables. While these equations are suitable for direct numerical simulation of turbulent flow, it is not possible to apply them directly in field studies. A more appropriate base for field studies is the Reynolds Averaged Navier-Stokes (RANS) equations (Monin & Yaglom, 1971; Dey, 2014), i.e.:

$$\frac{\partial \bar{u}}{\partial t} + \bar{u}\frac{\partial \bar{u}}{\partial x} + \bar{v}\frac{\partial \bar{u}}{\partial y} + \bar{w}\frac{\partial \bar{u}}{\partial z} = -\frac{1}{\rho}\frac{\partial \bar{p}}{\partial x} + \boldsymbol{\nu}\left(\frac{\partial^2 \bar{u}}{\partial x^2} + \frac{\partial^2 \bar{u}}{\partial y^2} + \frac{\partial^2 \bar{u}}{\partial z^2}\right) - \frac{\partial \overline{u'^2}}{\partial x} - \frac{\partial \overline{u'v'}}{\partial y} - \frac{\partial \overline{u'w'}}{\partial z} + g_x$$

$$\frac{\partial \bar{v}}{\partial t} + \bar{u}\frac{\partial \bar{v}}{\partial x} + \bar{v}\frac{\partial \bar{v}}{\partial y} + \bar{w}\frac{\partial \bar{v}}{\partial z} = -\frac{1}{\rho}\frac{\partial \bar{p}}{\partial y} + \boldsymbol{\nu}\left(\frac{\partial^2 \bar{v}}{\partial x^2} + \frac{\partial^2 \bar{v}}{\partial y^2} + \frac{\partial^2 \bar{v}}{\partial z^2}\right) - \frac{\partial \overline{u'v'}}{\partial x} - \frac{\partial \overline{v'^2}}{\partial y} - \frac{\partial \overline{v'w'}}{\partial z} + g_y$$

$$\frac{\partial \bar{w}}{\partial t} + \bar{u}\frac{\partial \bar{w}}{\partial x} + \bar{v}\frac{\partial \bar{w}}{\partial y} + \bar{w}\frac{\partial \bar{w}}{\partial z} = -\frac{1}{\rho}\frac{\partial \bar{p}}{\partial z} + \boldsymbol{\nu}\left(\frac{\partial^2 \bar{w}}{\partial x^2} + \frac{\partial^2 \bar{w}}{\partial y^2} + \frac{\partial^2 \bar{w}}{\partial z^2}\right) - \frac{\partial \overline{u'w'}}{\partial x} - \frac{\partial \overline{v'w'}}{\partial y} - \frac{\partial \overline{w'^2}}{\partial z} + g_z$$

where an overbar denotes a time (or ensemble) averaged quantity and prime denotes a deviation from the average quantity (e.g. $u = \overline{u} + u'$), $[u, v, w]$ are the three velocity components, $[x, y, z]$ are the three spatial directions (a right-handed coordinate system is used, see Figure 3 and Figure 5), ρ is fluid density, p is pressure, $\boldsymbol{\nu}$ is kinematic viscosity, g_i is the acceleration due to gravity in each direction (dependent on coordinate system

orientation), $\overline{u'_i u'_j}$ are the velocity variances and covariances (also known as the Reynolds turbulent stresses if a minus sign is added), $\frac{\partial}{\partial x_j}\left(-\overline{u'_i u'_j}\right)$ are the spatial gradients of the Reynolds stresses, and *i, j* are indices for the three spatial directions.

Spectral analysis provides a useful way to investigate the distribution of turbulent kinetic energy among frequencies, and to investigate periodic phenomena such as vortex shedding. Power spectral density (PSD) (also referred to as autospectral density) was computed using the periodogram method of Welch (1967), where the time series was divided into shorter subsections with 50% overlap, then PSD was computed for each of these subsections and ensemble averaged.

The shape of the probability density function of turbulent fluctuations was investigated using skewness, where $\mathrm{s}(u) = \overline{u'^3}/(\overline{u'^2})^{1.5}$. Evaluation of statistics such as skewness can help to detect infrequent high magnitude turbulence that may be due to physical interactions between flow and vegetation (Nikora *et al.*, 1997).

2.5. Vegetation measurements

The geometry of the studied macrophyte (Figure 4) was measured in-situ using tape measures and rulers. Canopy top, bottom, and width were measured at 20 cm intervals along the macrophyte centreline. Measurements were performed twice, with the operator standing on alternate sides of the macrophyte patch, and then measurements were averaged. Measurements of patch geometry were also performed for the trimmed patch configuration. After field investigations were completed the studied patch was transported to the laboratory, lightly dried with paper towels, then analysed to determine its mass, volume, density, stem length, and number of leaves and roots (Biggs, 2017).

Biometric data from another *R. penicillatus* patch from North East Scotland (River Urie) are provided for comparison, and to investigate whether the biometric properties of *R. penicillatus* patches are site specific. The patch from the River Urie was a median sized specimen from that river (Biggs *et al*., 2018). An aerial survey of the study reach (Figure 1) was also undertaken to quantify total patch cover and the geometry of the 125 *R. penicillatus* patches present. Surveying was performed using an Unmanned Aerial Vehicle (UAV) following the methods described by Biggs *et al*., (2018).

3. Results

3.1. Patch geometry and biometrics

There were 125 patches of *R. penicillatus* in the 100 m study reach of the Luther Water (Table 1). The total planform area of these patches was 184.89 m^2, compared to the total river planform area of 546.06 m^2, yielding a surface area blockage factor of 0.3386. The studied patch was 3.80 m long, 1.24 m wide and had tissue volume of 0.0198 m^3 in its natural configuration (Table 2). This corresponds to the 72nd percentile for length and the 83rd percentile for width compared to the other patches in the reach. In the trimmed configuration the patch was 2.4 m long, 0.71 m wide, and had tissue volume of 0.00415 m^3 (Table 2). This corresponds to the 36th percentile for length and the 60th percentile for width compared to the other patches in the reach, and 21% of the tissue volume of the natural patch. The density of the patch was 830.7 kgm^{-3} in its natural configuration and 862.7 kgm^{-3} in its trimmed configuration (Table 2).

3.2. Mean velocities

In the wake of the natural *R. penicillatus* patch (Figure 5a) streamwise mean velocities were greatly reduced compared to the rough bed control (Figure 5c). Depth averaged

streamwise mean velocity at x = 0 m, y = 0 m in P01 (i.e. 0.5 m downstream from the patch end and on the patch centerline) was only 50.8% of the value for the rough bed control. This effect was still apparent, but less severe, for the trimmed patch (Figure 5b), with depth averaged streamwise mean velocity at x = 0 m, y = 0 m in P13 reduced to 77.8% of the value for the rough bed control. The influence of the patch extended to the far wake (Figure 5d), with depth averaged streamwise mean velocity at x = 1.81 m, y = 0 m being 71.7% of the upstream rough bed control.

Vertical profiles of streamwise velocity in the patch's wake (Figure 6) did not follow the standard logarithmic profiles traditionally expected for an open-channel flow over rough beds. This was apparent both in the near-wake region (Figure 6a) and though less evident, in the far-wake region (Figure 6b). The spatial distribution of streamwise mean velocity in the patch wake (Figure 5a) indicated that flow was being redirected underneath the canopy. At locations such as y = -0.2 m or y = -0.4 m (Figure 6a) this resulted in peaks of streamwise mean velocity around 0.6 of depth.

3.3. Turbulent kinetic energy

The natural *R. penicillatus* patch caused substantial changes to turbulent kinetic energy (TKE) compared to the rough bed control (Figure 7a and Figure 7c). The most pronounced effects occurred in the lateral shear layer of the patch (y = -0.4 to -0.6 m), where TKE was substantially higher than that observed in the same location for the rough bed control (Figure 7c). However, TKE downstream from the patch's lateral shear layer was far lower than that recorded in regions close to the rough bed. In particular, a region of very high TKE can be observed near the bed (y = -0.8 to -1.0 m) (Figure 7a). This corresponds to the wake region of a cobble cluster, the effects of which are also evident as a region of lower streamwise mean velocity (Figure 5). In the far wake (Figure 7d) the

effects of the patch on TKE were minimal compared to TKE over the rough bed. There was not a substantial increase in TKE at the centre of the patch wake for the trimmed patch (Figure 7b) compared to the natural patch (Figure 7a).

3.4. Velocity covariance and spatial gradients of Reynolds stresses

Lateral turbulent mixing due to $\overline{u'v'}$ was an important process downstream from the patch's shear layer (y = -0.4 to -0.6 m) (Figure 8a), compared to the rough bed control (Figure 8c). For example, the magnitude of $\overline{u'v'}$ at x = 0 m, y = -0.5 m and z = 0.3 m was 17.76 times larger with the natural patch present than for the rough bed control. The trimmed patch (Figure 8b) also affected the spatial distribution of $\overline{u'v'}$ compared to the rough bed control, however interactions with the trimmed patch could not be fully assessed as its' shear layer did not pass directly through $P06_T$. The effect of the natural patch shear layer on $\overline{u'v'}$ was still apparent in the far wake (Figure 8d), although the magnitude had reduced. The rough bed also caused substantial changes to the spatial distribution and magnitude of $\overline{u'v'}$ that were unrelated to the vegetation patch (e.g. the region y < -0.6 m and z < 0.2 m, Figure 8a,d). The rough bed caused larger magnitude changes to $\overline{u'v'}$ than those attributed to the vegetation patch but at smaller spatial scales.

Vertical turbulent mixing due to $\overline{u'w'}$ was an important process directly downstream from the patch canopy (Figure 9a). This contrasts with the lateral mixing due to $\overline{u'v'}$ where the largest effects were observed downstream from the patch shear layer (Figure 8a). Vertical turbulent mixing due to $\overline{u'w'}$ was also important over the rough bed (Figure 9), although the measurement locations of $P06_T$ and $P06_R$ made it challenging to resolve vertical turbulent mixing behind the trimmed patch (Figure 9b), or to provide a rough bed control that was coincident with the high $\overline{u'w'}$ apparent in Figure 9a that was

centered around y = -0.4 m, z = 0.3 m. In the far wake (Figure 9d) the effect of the macrophyte patch on $\overline{u'w'}$ was scarcely visible and the rough bed dominated.

The cross-stream configuration of the PIV system provided the capability to resolve spatial gradients of Reynolds stresses in the y and z directions. This was very informative for the RANS x momentum equation and allowed average accelerations due to $-\partial\overline{u'v'}/\partial y$ and $-\partial\overline{u'w'}/\partial z$ to be explicitly determined (Figure 10). Downstream from the patch's shear layer (Figure 10a), $-\partial\overline{u'v'}/\partial y$ contributed distinct regions of positive mean acceleration (due to the lateral turbulent transportation of high momentum fluid from the shear layer into the wake), and negative mean acceleration (due to lateral turbulent transportation of low momentum fluid from the wake into the shear layer). Large scale mean accelerations due to $-\partial\overline{u'w'}/\partial z$ were also apparent in the wake of the patch, where a zone of positive mean acceleration occurred near the surface due to high momentum fluid from under the canopy being transported towards the surface. Likewise, a large zone of negative mean acceleration was present underneath the canopy due to low momentum fluid from behind the bulk of the patch's biomass being transported lower in the water column. Mean accelerations due to turbulent mixing downstream from the patch were not substantial in the far wake (Figure 10b,d). The rough bed contributed high magnitude mean accelerations, but at a smaller spatial scale; for example, very strong mean accelerations due to $-\partial\overline{u'v'}/\partial y$ and $-\partial\overline{u'w'}/\partial z$ were observed in the wake of the cobble cluster (y = -0.8 to -1.0 m) (Figure 10a,c).

The velocity covariance $\overline{v'w'}$ was generally an order of magnitude less important than $\overline{u'v'}$ or $\overline{u'w'}$ and is not presented here. The spatial gradient of the $-\overline{u'^2}$ normal stress (e.g. $-\partial\overline{u'^2}/\partial x$) could not be determined for cross stream measurement planes and may

have contributed significantly to mean accelerations in the x direction. The spatial gradients of the normal stresses in the y and z momentum equations (e.g. $-\partial\overline{v'^2}/\partial y$ and $-\partial\overline{w'^2}/\partial z$) provided significant contributions to mean accelerations in the y and z directions, compared to $-\partial\overline{v'w'}/\partial y$ and $-\partial\overline{v'w'}/\partial z$. The terms $-\partial\overline{u'v'}/\partial x$ and $-\partial\overline{u'w'}/\partial x$ could not be resolved for the cross-stream measurement planes and may have provided significant mean accelerations in the y and z directions. Mean accelerations due to viscous stresses (e.g. $\boldsymbol{\nu}\Delta\overline{u_i}$) were two orders of magnitude lower than those for turbulent stresses and are not shown here.

3.5. Velocity spectra and skewness

For the flow conditions studied, velocity spectra provided no indication of periodic phenomena such as periodic vortex formation in the wake or downstream from the patch's shear layer. This is illustrated by the spectra at x = 0 m, y = -0.5 m, z = 0.3 m in P06 (Figure 11a) and at x = 1.81 m, y = -0.5 m, z = 0.3 m in P18 (Figure 11b).

The skewness of u (Figure 12a,b) indicated that the distribution of turbulent fluctuations was skewed by low streamwise velocity events above the rough bed (y = -0.6 to -1.1 m), and high streamwise velocity events in the wake of the patch (y = 0 to -0.5 m). The skewness of v (Figure 12c,d) was strongly positive in the patch wake, which indicates that the distribution of cross stream turbulent fluctuations in the patch wake was skewed by high magnitude positive events (likely originating from the patch shear layer).

3.6. Sedimentation

Deposition of sediment was observed within the front part of the patch (where it connects to the bed) (Figure 13), but only a small accumulation of fine sediment was observed in the wake, or underneath the floating canopy. This differs from the wake of some other

macrophytes in the river reach, where large mounds of accumulated sediment were observed underneath the canopy. However, these other macrophytes were generally larger, in shallower water and had their canopies close to the river bed.

4. Discussion

4.1. Macrophyte geometry and biometrics

The *R. penicillatus* patches in the Luther Water had a similar size distribution (Table 1) to patches in the River Urie (Biggs *et al*., 2018), indicating that size distributions of macrophyte species may generalise across geographic areas. Likewise, the density of the trimmed Luther Water macrophyte (Table 2) was comparable to a submerged patch of *R. penicillatus* from the River Urie (873.1 kgm^{-3}; Biggs *et al*., 2016). The density difference between the natural and trimmed patch configurations was likely due to the removal of positively buoyant trailing stems during trimming. The abundance of adventitious roots was substantially different between the two specimens (Table 2), and the Luther Water specific root value was only 51.6% of that found for the patch from the River Urie. There were also fewer leaves on the patch from the Luther Water. The average stem diameter of the Luther Water patch was slightly larger, although both specimens had similar specific stem length (Table 2).

Differences in the geometry and biometrics of the studied macrophyte from the Luther Water, and the specimen from the River Urie, may be due to the hydraulic conditions of their habitats. The River Urie macrophyte was from a higher stress environment (e.g. higher mean velocities and TKE (Biggs *et al*., 2016)), where it was

predominantly submerged and moved substantially with flow, whereas the Luther Water macrophyte had biomass concentrated at the water surface and moved little with flow.

Studying macrophytes *in situ* enables natural macrophyte morphology and hydraulic conditions to be investigated. This has many advantages compared to using geometric analogues (or surrogates), where flow conditions and macrophyte geometry should be scaled to represent realistic field conditions. At the end of the growing season, median patches of *R. penicillatus* had over 1 km of total stem length (Table 2). This is two to three orders of magnitude larger total stem length than the patch analogues of Siniscalchi *et al.,* (2010) and Siniscalchi & Nikora (2012), resulting in much larger magnitude velocity reductions in the wake of natural patches. Due to the difficulties of upscaling flow-vegetation interactions (e.g. total drag force is not the sum of component drag due to clumping and reconfiguration (Albayrak *et al*., 2014)), it remains to be determined whether small-scale lab measurements with patch analogues can be used to make realistic predictions of the flow downstream from natural patches at field-scales.

4.2. Mean velocities

The velocity distribution and substantial reduction in mean velocities observed in the wake of the *R. penicillatus* patch can most likely be attributed to the fact that the majority of the plant's biomass was near the water surface (Figure 4). Velocity reductions behind vegetation biomass and flow redirection under the canopy have also been reported in studies where biomass was concentrated higher in the water column (Boothroyd *et al*., 2017; Siniscalchi *et al*., 2012). Peaks of streamwise mean velocity in the patch wake occurred at approximately 0.6 of depth (Figure 6). This illustrates some of the potential problems that can be encountered when using simple discharge gauging techniques that rely on logarithmic velocity profiles (e.g. assuming that depth averaged velocity occurs

at 0.6 of depth). In vegetated rivers discharge gauging should use vertical profiles comprised of multiple measurements throughout the water column.

4.3. Turbulent kinetic energy

Increases in TKE were observed downstream from the patch shear layer (Figure 7a), but not directly downstream from the patch where TKE was low. This surprising pattern was also apparent for the trimmed patch (Figure 7b). In contrast, Siniscalchi, (2012) and Nikora *et al*., (2012) found enhanced TKE behind shoots or small plants/patches. This difference may illustrate the effects of vegetation scale and dynamics. Both the full size and trimmed patch in the Luther Water were wide, porous, did not move substantially, and had low TKE in their wake. This is similar to the results of Boothroyd *et al*., (2016) who found enhanced TKE in the downstream shear layer, but low TKE in the wake for the flow conditions investigated. Likewise, Cameron *et al*., (2013) found the highest TKE downstream from the canopy top shear layer (for a small macrophyte patch measured *in situ*), rather than directly in the patch wake. Biggs *et al*., (2016) investigated the flow around a 2.60 m long by 0.53 m wide patch of *R. penicillatus* (Table 2), with hydraulic conditions that induced substantial motion of the patch. They found that TKE was enhanced across most of the patch wake (especially downstream from the patch lateral shear layers), although there was still a small zone of low TKE at the centre of the patch wake. This indicates the importance of vegetation scale, geometry (e.g. aspect ratio) and dynamics for downstream turbulence. The size of the patch studied by Biggs *et al*., (2016) was representative of median *R. penicillatus* patches toward the end of the summer growing season (Biggs *et al*., 2018). The effects of patch size and geometry indicates that laboratory studies of flow-macrophyte interactions should use great care that replica vegetation is representative of natural patches (Biggs *et al.*, 2018).

4.4. Velocity covariance and spatial gradients of Reynolds stresses

In general, the patch caused low magnitude changes to $\overline{u'v'}$ over large spatial scales while the rough bed caused high magnitude changes to $\overline{u'v'}$ over small spatial scales (e.g. the wake of the cobble cluster in Figure 8a, and wakes of other cobbles in Figure 8d). The positive sign of $\overline{u'v'}$ downstream from the patch's shear layer (Figure 8a) indicates turbulent transportation of high momentum fluid from the shear layer into the wake and turbulent transportation of low momentum fluid from the wake into the shear layer. Further information on turbulent mixing can be deduced from the sign of $\overline{u'w'}$. Downstream from the macrophyte canopy (Figure 9a) $\overline{u'w'}$ was positive. This indicates upwards turbulent transportation of higher momentum fluid (e.g. flow from under the macrophyte being transported towards the surface) and downwards turbulent transportation of lower momentum fluid (e.g. flow from near the surface and behind the concentration of macrophyte biomass being transported toward the bed). This positive sign contrasts with the negative value of $\overline{u'w'}$ which is common over rough beds (Figure 9a,d) and occurs due bursting phenomena such as sweeps and ejections. The roughness of the bed no doubt influenced the spatial distribution of $\overline{u'v'}$ and $\overline{u'w'}$, however the advantage of studying natural macrophyte patches in their natural habitats is that bed roughness is not prescribed but evolves over the growing season as macrophyte biomass changes (e.g. substrate and macrophytes are a coupled system due to flow redirection around and between patches).

The importance of turbulent momentum fluxes downstream from the patch was particularly apparent where faster moving fluid from adjacent areas (Figure 8a), or flowing under the patch (Figure 9a), interacted with slow fluid in the patch wake. For the

large patch studied in the Luther Water, the magnitude of $\overline{u'v'}$ was larger than $\overline{u'w'}$ in the patch wake. However, the magnitude of mean accelerations due to vertical mixing $|-\partial\overline{u'w'}/\partial z|$ were slightly larger than those due to horizontal mixing $|-\partial\overline{u'v'}/\partial y|$, since $\overline{u'w'}$ had a stronger vertical gradient. In rivers $\left|\overline{u'w'}\right|$ is usually substantially larger than $\left|\overline{u'v'}\right|$ since vertical momentum exchange due to flow resistance from the rough bed dominates. This can be observed in the region beside the patch and above the rough bed (e.g. y < -0.6 m in Figure 8a,d and Figure 9a,d). The result that $\left|\overline{u'v'}\right| > \left|\overline{u'w'}\right|$ in the patch wake (downstream from the lateral shear layer) shows the importance of lateral mixing for flow around 3D porous obstructions such as macrophytes (Biggs *et al*., 2016).

4.5. Velocity spectra and skewness

The formation of a vortex street behind the patch of *R. penicillatus* was not observed within the available measurement domain. This may be due to the porosity of the patch (Taddei *et al*., 2016) delaying the onset of a vortex street (Zong & Nepf, 2012; Hu *et al*., 2018) until further downstream than field measurements were feasible with the PIV system. It is possible that both the near and far wake regions (Figure 3) corresponded to the steady wake region observed by Zong & Nepf (2012). This would explain why periodic turbulent fluctuations with patch width scale were not observed in the far wake measurement planes (Figure 11b). However, this explanation needs experimental verification, since the geometry of the natural *R. penicillatus* patch is very different to the circular cylinder array with two dominant length scales used by Zong & Nepf (2012). Spectral peaks that correspond to the scale of patch length were also not observed (e.g. Figure 11 and spectra at other locations in the measurement planes). This contrasts with the results found for flow behind a small (0.4 m long) natural patch of *R. penicillatus*

(Cameron *et al*., 2013). The difference may be due to the motion of the small patch, which moved with a characteristic frequency of ~1 Hz. This corresponded to large eddies with similar scale to flow depth or patch length, whereas the large (3.8 m long) patch in this study moved little at the flow conditions investigated.

The distinct lack of redistribution of energy to higher frequency turbulence in the macrophyte wake was notable compared to Zong & Nepf (2012) who reported a redistribution of energy to stem-scale turbulence behind their replica patch. Cameron *et al*., (2013) found higher TKE in the wake of their patch compared to flow in the free stream above the patch. This difference in TKE manifested as a concentration of energy between 0.5 and 1 Hz (which was not present in the free stream above the patch) and increased energy of high frequency turbulence. The lack of energy redistribution in the present study may be because the near wake PIV planes were too far downstream (0.5 m from the end of a 3.8 m long macrophyte patch) and fine scale turbulence had already dissipated by the time it reached the measurement planes. However, it was not possible to measure closer to the end of the vegetation canopy without causing interference. Thus, the measurement locations may have fallen into a zone corresponding to the middle of the steady wake region, where neither large scale patch turbulence nor small scale stem and leaf turbulence could be resolved.

It is currently unknown whether macrophytes flap only in response to incoming turbulence, as observed for small plant samples by Siniscalchi & Nikora (2013), or whether larger macrophytes experience a coupling between vortex shedding and patch oscillations, where the downstream instability triggers plant motion. It is possible that the summer discharge during the PIV deployment was too low to see the full effect of natural

macrophytes on the generation of large scale turbulence. Vigorous flapping, dynamic reconfiguration and highly turbulent wakes were observed behind these large macrophytes during flood events, but due to the need for stability and problems caused by high turbidity, performing field experiments with PIV during floods is not currently possible. Thus, the high energy flows that are the most important factor defining bed morphology and hydraulic control of macrophytes (Franklin *et al*., 2008) cannot easily be studied, so these processes and interactions must be extrapolated from lower discharge conditions. This issue is common to many questions in ecohydrology (e.g. understanding the implications of high discharge for benthic invertebrates) and requires further technical developments to enhance measurement capabilities, or advances in numerical simulation of flow interactions with flexible vegetation (e.g. Marjoribanks *et al*., 2017; Boothroyd *et al*., 2017; Tschisgale *et al*., 2017).

The positive skewness of u observed touching the rough bed (Figure 12a,b) was likely due to sweeps, while the negative skewness of u slightly above the rough bed was likely due to ejections. The large zone of negative skewness further above the rough bed (near the top of the water column) is somewhat harder to interpret. This may be due to large scale phenomena such as changing flow paths through the patch mosaic, or surge flow across the whole channel due to the dynamic resistance of aquatic vegetation. The positive skewness of u in the wake of the patch (Figure 12a,b) was likely due to the transportation of higher momentum fluid from underneath the patch by $\overline{u'w'}$ in the near wake (Figure 9a), and from beside the patch by $\overline{u'v'}$ in both near and far wake (Figure 8a,d). The positive skewness of v in the patch wake was particularly apparent in the far wake (Figure 12d) and may be the start of a von Kármán vortex street which has been

delayed by patch porosity (Zong & Nepf, 2012; Chang & Constantinescu, 2015; Hu *et al*., 2018).

4.6. Sedimentation

Sedimentation within aquatic vegetation is influenced by stem density (Bouma *et al*., 2007), patch size (Zong & Nepf, 2011) and the presence of flexible leaves (Hu *et al*., 2018). Sedimentation at the upstream end of the macrophyte patch (Figure 13) was likely caused by the high stem density of the *R. penicillatus* patch where it contacted the bed (Figure 3). The lack of significant sedimentation underneath and behind the studied patch may be due to flow redirection underneath the positively buoyant canopy (Figure 5). It is also possible that the accumulation of sediment at the upstream end of the patch (Figure 13) forms a 'bluff body' that is large enough to generate substantial downstream turbulence (e.g. underneath the macrophyte patch) to avoid further sedimentation. Sedimentation is routinely observed within real aquatic vegetation (Sand-Jensen, 1998; Schulz *et al*., 2003; Jones *et al*., 2012 and references therein), however this phenomenon is not well captured by some laboratory experiments (Follett & Nepf, 2012). This highlights the importance of field work to investigate sediment transport around aquatic vegetation.

5. Conclusions

High-resolution measurements of flow velocities in the wake of a patch of *R. penicillatus* were successfully obtained by using stereoscopic PIV in the field. Macrophyte biomass was positively buoyant and was concentrated near the water surface, with substantial reductions to mean velocities in its wake. Flow was redirected under the macrophyte

canopy, resulting in velocity profiles that were not logarithmic, with peak velocities around 0.6 of depth. This has implications for any work in vegetated rivers (e.g. discharge gauging) that assumes a single measurement location at 0.6 of depth provides an estimate of mean velocity. Turbulent kinetic energy was enhanced in the patch shear layer, but not in the wake directly behind the patch. This may be due to a lack of vegetation motion at the summer flow conditions investigated, or it may be due to fine scale turbulence being dissipated before it reached the PIV measurement planes. Lateral and vertical turbulent mixing were both important processes in the patch wake, with higher momentum fluid from beside the patch (and under the canopy) mixing with lower momentum fluid from near the water surface (e.g. downstream from the canopy where biomass was concentrated near the water surface). Large scale periodic coherent structures (such as Kelvin Helmholtz or von Kármán vortices) were not detected within the measurement domain. This may be due to the low-energy flow conditions investigated (which did not induce vegetation motion), or vegetation porosity delaying vortex street formation until further downstream than our measurement domain.

Measurements of patch geometry and biometrics were informative, as they illustrated many difference between the *Ranunculus* morphotype (which is common in rivers and streams globally), and geometric analogues such as rigid cylinder arrays, or replica submerged flexible patches (e.g. different buoyancy, biomass distributions, patch length, aspect ratio, total stem length, total leaves and total surface area). Rigid cylinder arrays provide a good analogue for mangroves or emergent reedy vegetation, but it is challenging to directly compare results with natural patches that are highly flexible, spatially complex, and have different drag characteristics (e.g. viscous drag will be significantly more important for natural macrophytes than for rigid cylinder arrays). It is

hoped that the data on macrophyte geometry and biometrics presented here will assist with the design of more realistic replicas for use in laboratory studies.

Acknowledgements

The authors would like to thank: Jochen Aberle, Alexander Sukhodolov and Bernhard Statzner for valuable discussions and advice during the project; Alasdair Matheson and the Scottish Environment Protection Agency (SEPA) for providing discharge and river stage data; the journal editors and two anonymous reviewers for comments and suggestions that significantly improved the paper.

Disclosure statement

There are no known conflicts of interest related to the work.

Funding

The work was part of the research project 'Hydrodynamic Transport in Ecologically Critical Heterogeneous interfaces' (HYTECH), the support of which, under the European Union's Seventh Framework Programme (Marie Curie FP7-PEOPLE-2012-ITN, European Commission grant agreement number 316546), is gratefully acknowledged. The work was also partially funded by the National Institute of Water and Atmospheric Research (NIWA) under the Sustainable Water Allocation Research Programme (CDPD1706), the support of which is gratefully acknowledged.

References

Abdolahpour, M., Ghisalberti, M., McMahon, K., Lavery, P. (2018). The impact of flexibility on flow, turbulence, and vertical mixing in coastal canopies. Limnology and Oceanography, 63(6), 2777-2792.

Albayrak, I., Nikora, V., Miler, O., O'Hare, M. (2012). Flow-plant interactions at a leaf scale: effects of leaf shape, serration, roughness and flexural rigidity. Aquatic Sciences, 74(2), 267-286.

Albayrak, I., Nikora, V., Miler, O., O'Hare, M. (2014). Flow–plant interactions at leaf, stem and shoot scales: drag, turbulence, and biomechanics. Aquatic Sciences, 76(2), 269-294.

Bal, K., Meire, P. (2009). The influence of macrophyte cutting on the hydraulic resistance of lowland rivers. Journal of Aquatic Plant Management, 47(1), 65-68.

Biggs, H., Nikora, V., Papadopoulos, K., Vettori, D., Gibbins, C., Kucher, M. (2016). Flow-vegetation interactions: A field study of Ranunculus penicillatus at the large patch scale. Proceedings of the 11th International Symposium on Ecohydraulics, Melbourne, Australia.

Biggs, H. (2017). Flow-vegetation interactions: from the plant to the patch mosaic scale (Doctoral dissertation). University of Aberdeen, Aberdeen, United Kingdom.

Biggs, H., Nikora, V., Gibbins, C., Fraser, S., Papadopoulos, K., Green, D., Hicks, M. (2018). Coupling Unmanned Aerial Vehicle (UAV) and hydraulic surveys to study the geometry and spatial distribution of aquatic macrophytes. Journal of Ecohydraulics, 3(1), 45-58.

Boothroyd, R., Hardy, R., Warburton, J., Marjoribanks, T. (2016). The importance of accurately representing submerged vegetation morphology in the numerical prediction of complex river flow. Earth Surface Processes and Landforms, 41(4), 567-576.

Boothroyd, R., Hardy, R., Warburton, J., Marjoribanks, T. (2017). Modelling complex flow structures and drag around a submerged plant of varied posture. Water Resources Research, 53(4), 2877-2901.

Bouma, T., Van Duren, L., Temmerman, S., Claverie, T., Blanco-Garcia, A., Ysebaert, T., Herman, P. (2007). Spatial flow and sedimentation patterns within patches of epibenthic structures: Combining field, flume and modelling experiments. Continental Shelf Research, 27(8), 1020-1045.

Butcher, R. (1933). Studies on the ecology of rivers: I. On the distribution of macrophytic vegetation in the rivers of Britain. The Journal of Ecology, 21(1), 58-91

Cameron, S. (2011). PIV algorithms for open-channel turbulence research: accuracy, resolution and limitations. Journal of Hydro-environment Research, 5(4), 247-262.

Cameron, S., Nikora, V., Albayrak, I., Miler, O., Stewart, M., Siniscalchi, F. (2013). Interactions between aquatic plants and turbulent flow: a field study using stereoscopic PIV. Journal of Fluid Mechanics, 732(1), 345-372.

Chang, K., Constantinescu, G. (2015). Numerical investigation of flow and turbulence structure through and around a circular array of rigid cylinders. Journal of Fluid Mechanics, 776(1), 161-199.

Dawson, F. (1989). Ecology and management of water plants in lowland streams. Freshwater Biology Annual Report, 57(1), 43-60.

Dey, S. (2014). Fluvial hydrodynamics. Berlin: Springer.

Figueiredo, B., Mormul, R., Thomaz, S. (2015). Swimming and hiding regardless of the habitat: prey fish do not choose between a native and a non-native macrophyte species as a refuge. Hydrobiologia, 746(1), 285–290.

Folkard, A. (2011). Vegetated flows in their environmental context: a review. Proceedings of the Institution of Civil Engineers - Engineering and Computational Mechanics, 164(1), 3-24.

Follett, E., Nepf, H. (2012). Sediment patterns near a model patch of reedy emergent vegetation. Geomorphology, 179(1), 141-151.

Franklin, P., Dunbar, M., Whitehead, P. (2008). Flow controls on lowland river macrophytes: a review. Science of the Total Environment, 400(1), 369-378.

Garner, P., Bass, J., Collett, G. (1996). The effects of weed cutting upon the biota of a large regulated river. Aquatic Conservation: Marine and Freshwater Ecosystems, 6(1), 21-29.

Greer, M., Hicks, A., Crow, S., Closs, G. (2017). Effects of mechanical macrophyte control on suspended sediment concentrations in streams. New Zealand Journal of Marine and Freshwater Research, 51(2), 254-278.

Gurnell, A., Van Oosterhout, M., De Vlieger, B., Goodson, J. (2006). Reach-scale interactions between aquatic plants and physical habitat: River Frome, Dorset. River Research and Applications, 22(6), 667-680.

Hu, Z., Lei, J., Liu, C., Nepf, H. (2018). Wake structure and sediment deposition behind models of submerged vegetation with and without flexible leaves. Advances in Water Resources, 118(1), 28-38.

Jones, J., Collins, A., Naden, P., Sear, D. (2012). The relationship between fine sediment and macrophytes in rivers. River Research and Applications, 28(7), 1006-1018.

Kemp, P., Sear, D., Collins, A., Naden, P., Jones, I. (2011). The impacts of fine sediment on riverine fish. Hydrological Processes, 25(11), 1800-1821.

Madsen, J., Chambers, P., James, W., Koch, E., Westlake, D. (2001). The interaction between water movement, sediment dynamics and submersed macrophytes. Hydrobiologia, 444(1-3), 71-84.

Marjoribanks, T., Hardy, R., Lane, S., Tancock, M. (2017). Patch-scale representation of vegetation within hydraulic models. Earth Surface Processes and Landforms, 42(5), 699-710.

Monin, A., Yaglom, A. (1971). Statistical fluid mechanics: Mechanics of turbulence (Volumes 1 & 2). Courier Corporation.

Nepf, H. (2012). Hydrodynamics of vegetated channels. Journal of Hydraulic Research, 50(3), 262-279.

Nikora, V., Goring, D., Biggs, B. (1997). On stream periphyton-turbulence interactions. New Zealand Journal of Marine and Freshwater Research, 31(4), 435-448.

Nikora, V. (2010). Hydrodynamics of aquatic ecosystems: an interface between ecology, biomechanics and environmental fluid mechanics. River Research and Applications, 26(4), 367-384.

Nikora, V., Cameron, S., Albayrak, I., Miler, O., Nikora, N., Siniscalchi, F., O'Hare, M. (2012). Flow-biota interactions in aquatic systems: scales, mechanisms and challenges. In Rodi W. & Uhlmann M. (Ed.) Environmental Fluid Mechanics: Memorial Volume in Honour of Prof. Gerhard H. Jirka, 217-235.

Nishihara, G., Ackerman, J. (2006). The effect of hydrodynamics on the mass transfer of dissolved inorganic carbon to the freshwater macrophyte Vallisneria americana. Limnology and Oceanography, 51(6), 2734-2745.

Raffel, M., Willert, C., Wereley, S., Kompenhans, J. (2007). Particle image velocimetry: a practical guide. 2nd Ed. Springer.

Rominger, J., Nepf, H. (2011). Flow adjustment and interior flow associated with a rectangular porous obstruction. Journal of Fluid Mechanics, 680(1), 636-659.

Sand-Jensen, K. (1998). Influence of submerged macrophytes on sediment composition and near-bed flow in lowland streams. Freshwater Biology, 39(4), 663-679.

Schulz, M., Kozerski, H., Pluntke, T., Rinke, K. (2003). The influence of macrophytes on sedimentation and nutrient retention in the lower River Spree (Germany). Water Research, 37(3), 569-578.

Shupryt, M., Stelzer, R. (2009). Macrophyte beds contribute disproportionately to benthic invertebrate abundance and biomass in a sand plains stream. Hydrobiologia, 632(1), 329-339.

Siniscalchi, F., Nikora, V., Cameron, S., Lacey, R., Marion, A. (2010). Flow-vegetation interaction at a scale of individual plant: a case study of Ranunculus penicillatus. Proceedings of Riverflow 2010, (pp. 445-451), Braunschweig, Germany.

Siniscalchi, F. (2012). Hydrodynamics of flow-vegetation interactions at the scales of individual plant and plant patch (Doctoral dissertation). University of Aberdeen, Aberdeen, United Kingdom.

Siniscalchi, F., Nikora, V., Aberle, J. (2012). Plant patch hydrodynamics in streams: Mean flow, turbulence, and drag forces. Water Resources Research, 48(1), 1-14.

Siniscalchi, F., Nikora, V. (2012). Flow-plant interactions in open-channel flows: A comparative analysis of five freshwater plant species. Water Resources Research, 48(5), 1-13.

Siniscalchi, F., Nikora, V. (2013). Dynamic reconfiguration of aquatic plants and its interrelations with upstream turbulence and drag forces. Journal of Hydraulic Research, 51(1), 46-55.

Stamhuis, E. (2006). Basics and principles of particle image velocimetry (PIV) for mapping biogenic and biologically relevant flows. Aquatic Ecology, 40(4), 463-479.

Stewart, M. (2014). Turbulence structure of rough-bed open-channel flow (Doctoral dissertation). University of Aberdeen, Aberdeen, United Kingdom.

Taddei, S., Ganapathisubramani, B., Manes, C. (2016). Characterisation of drag and wake properties of canopy patches immersed in turbulent boundary layers. Journal of Fluid Mechanics, 798(1), 27-49.

Tschisgale, S., Meller, R., Frohlich, J. (2017). Simulation of the turbulent flow over an array of flexible blades. Proceedings of the Tenth International Symposium on Turbulence and Shear Flow Phenomena, Chicago, USA.

Welch, P. (1967). The use of fast Fourier transform for the estimation of power spectra: A method based on time averaging over short, modified periodograms. IEEE Transactions on Audio and Electroacoustics, 15(2), 70-73.

Zong, L., Nepf, H. (2011). Spatial distribution of deposition within a patch of vegetation. Water Resources Research, 47(3), 1-12.

Zong, L., Nepf, H. (2012). Vortex development behind a finite porous obstruction in a channel. Journal of Fluid Mechanics, 691(1), 368-391.

Tables and figures

Table 1. Geometry of the 125 *Ranunculus penicillatus* patches found in the study reach of the Luther Water. Mean data are provided, as well as quartiles from the cumulative distribution function, where 0% is the minimum, 50% is the median, 100% is the maximum and 75% - 25% is the interquartile range.

Parameter	Mean	0%	25%	50%	75%	100%
Planform area (m^2)	1.479	0.01	0.27	0.86	2.21	6.92
Length (m)	3.051	0.25	1.93	2.92	3.94	7.00
Width (m)	0.7000	0.05	0.25	0.52	1.08	2.19
Aspect ratio	7.447	2.10	3.91	6.13	9.78	22.00

Table 2. Biometrics of the *R. penicillatus* patch from the Luther Water in its natural and trimmed configuration, with comparison to a *R. penicillatus* patch from the River Urie.

	Luther Water, Natural Macrophyte August 2015	Luther Water, Trimmed Macrophyte August 2015	River Urie, Natural Macrophyte September 2014
Area (m^2)	3.18	1.15	1.05
Length (m)	3.80	2.40	2.60
Width (m)	1.24	0.710	0.530
Aspect ratio	3.06	3.37	4.91
Tissue volume (lab, m^3)	0.0198	0.00415	0.00702
Tissue mass (lab, kg)	16.460	3.580	6.133
Tissue density (lab, kgm^{-3})	830.7	862.7	873.1
Specific leaves (leaves/g)	1.964		2.785
Specific roots (roots/g)	0.7045		1.366
Specific stem length (m/g)	0.1883		0.1986
Average stem diameter (mm)	2.19		1.94
Extrapolated total leaves	32330	7032	17080
Extrapolated total roots	11600	2522	8378
Extrapolated total stem length (m)	3099	674	1218

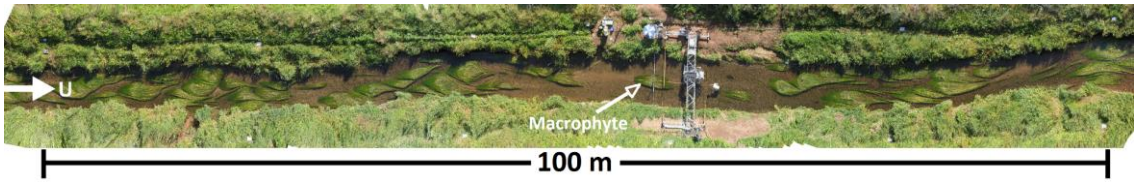

Figure 1. Study reach in the Luther Water (NE Scotland, UK), site coordinates N 56.832, E -2.498.

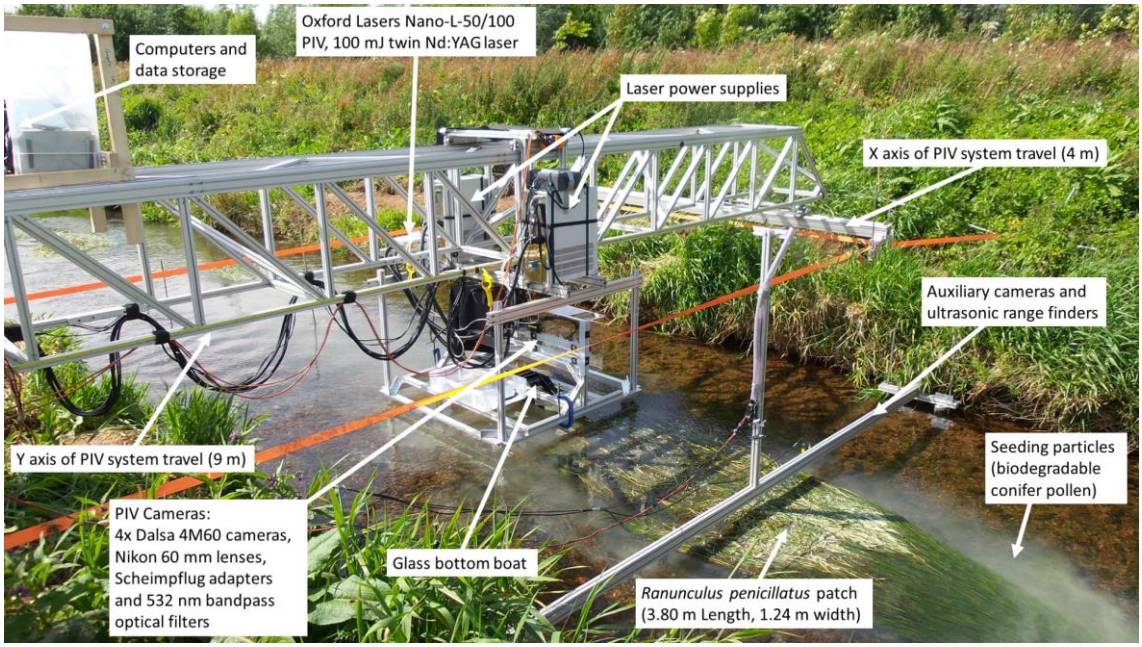

Figure 2. Stereoscopic Particle Image Velocimetry field system in the Luther Water.

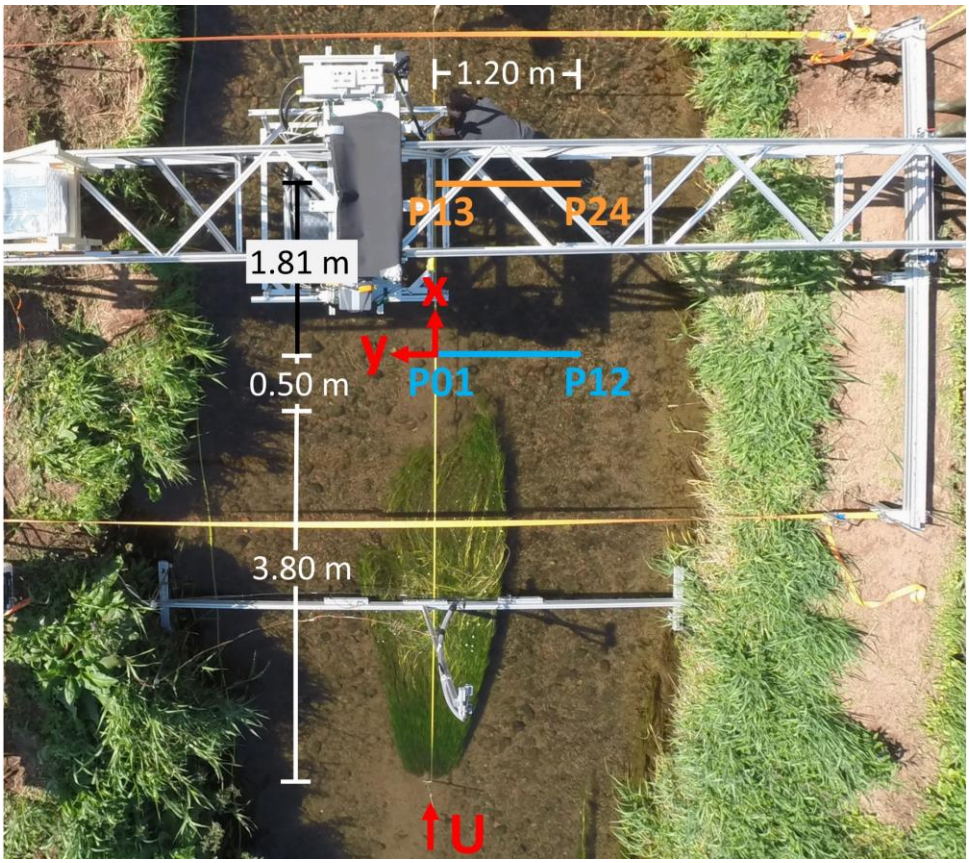

Figure 3. PIV measurements planes: P01 to P12 in the near wake, P13 to P24 in the far wake. After the macrophyte was trimmed $P01_T$ and $P06_T$ were repeated, then after the macrophyte was removed $P01_R$ and $P06_R$ were repeated as a rough bed control. A right-handed coordinate system was used, the origin of which coincided with the centreline of the macrophyte patch and plane P01.

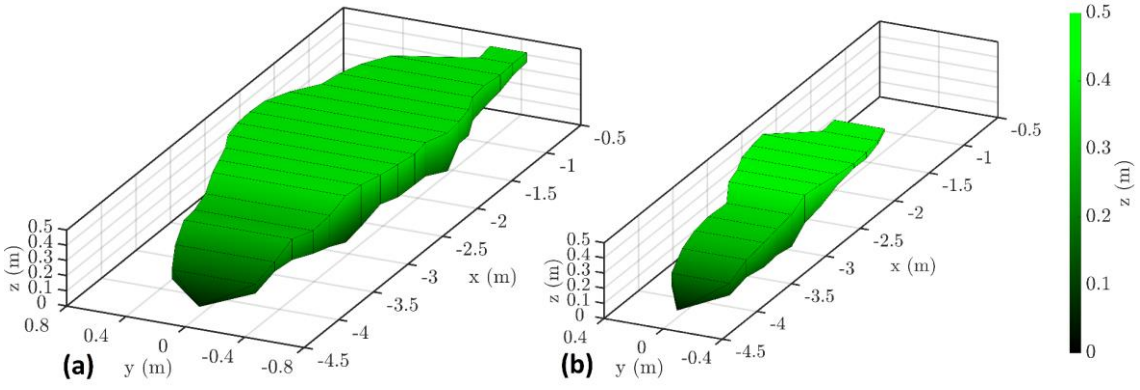

Figure 4. Geometry of: (a) natural macrophyte patch with projected frontal area 0.376 m^2 and planform area 3.184 m^2; (b) trimmed macrophyte patch with projected frontal area 0.181 m^2 and planform area 1.151 m^2. The patch was also removed completely as a rough bed control.

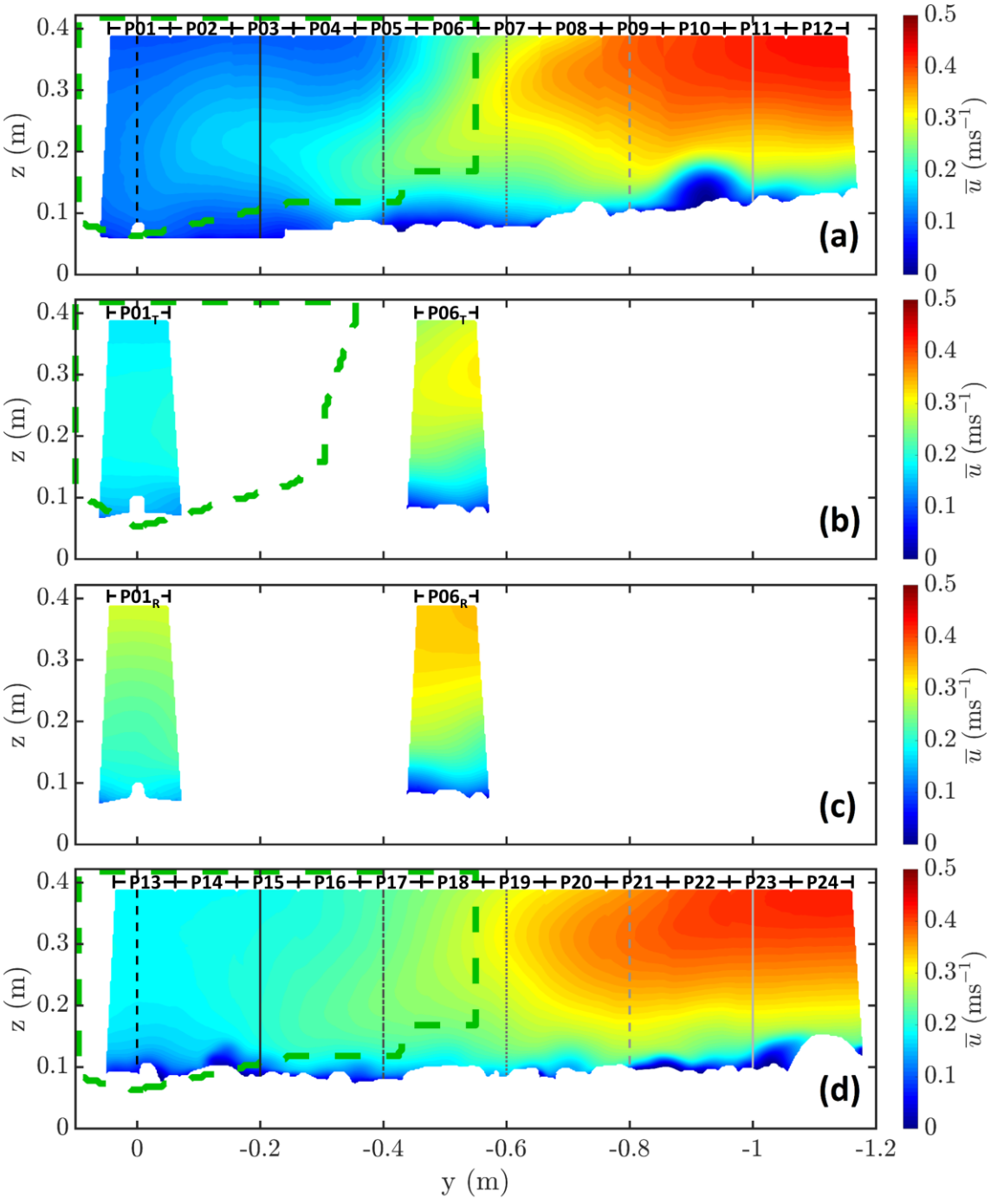

Figure 5. Streamwise mean velocity: (a) P01 to P12 in the near wake of the natural patch of *R. penicillatus*; (b) $P01_T$ and $P06_T$ for the trimmed patch; (c) $P01_R$ and $P06_R$ for the rough bed control; (d) P13 to P24 in the far wake of the natural patch. The green dashed lines are the downstream projection of the patch boundaries. The vertical lines on (a) and (d) correspond to velocity profiles shown in the subsequent figure. A right-handed coordinate system was used throughout the study and subsequent analysis.

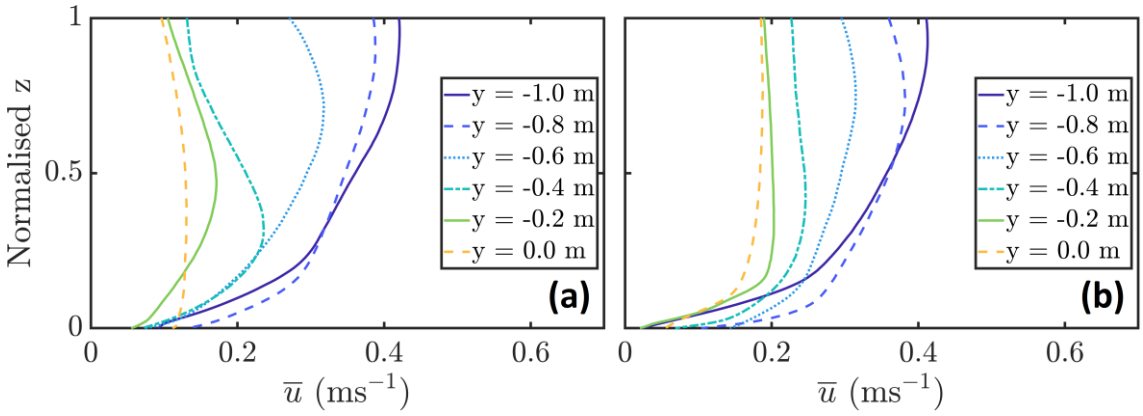

Figure 6. Vertical profiles of streamwise mean velocity from figure 5: (a) near wake of the natural macrophyte; (b) far wake of the natural macrophyte. Profile elevations are normalised by the distance from the water surface to the masked river bed.

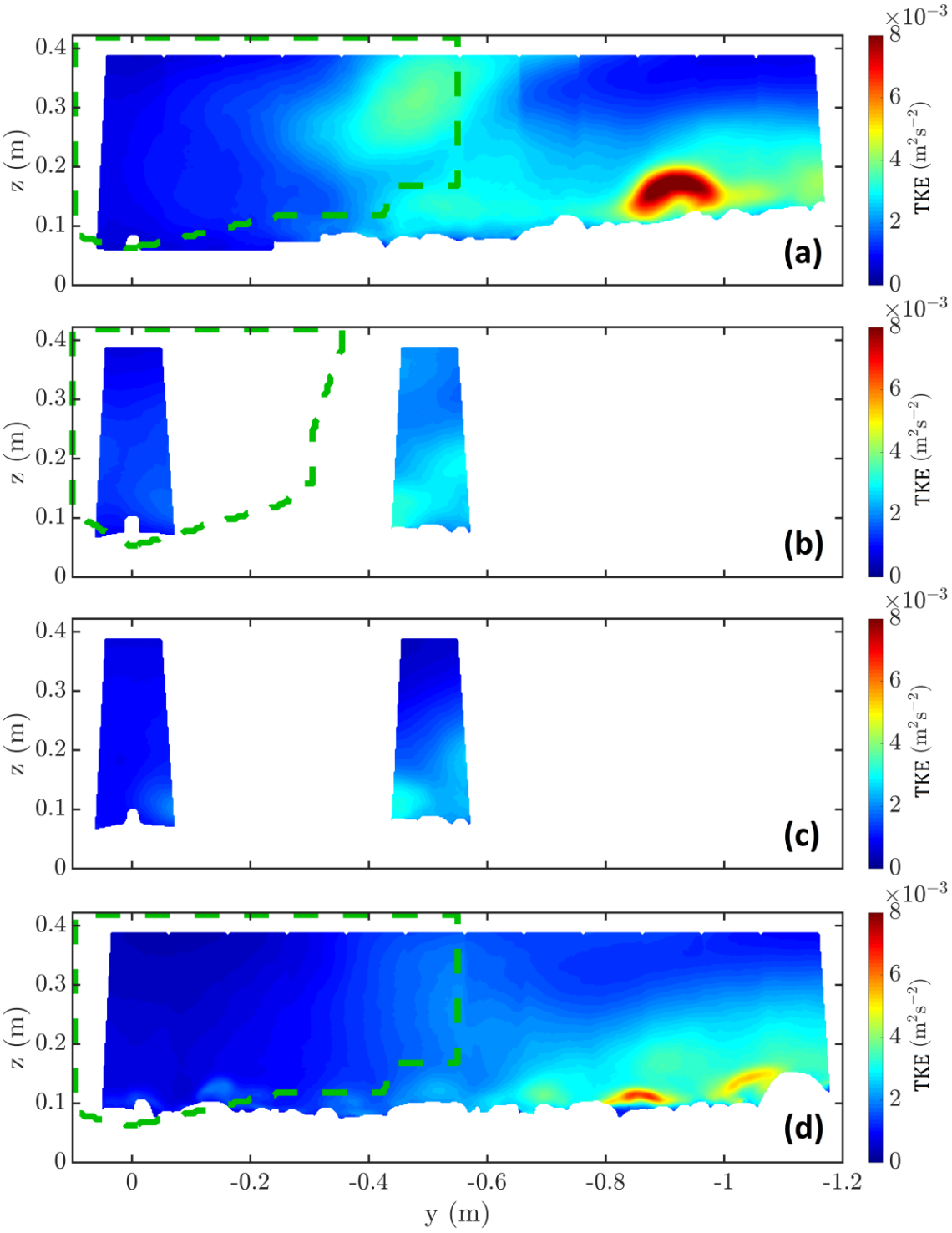

Figure 7. Turbulent kinetic energy $0.5\left(\overline{u'^2}+\overline{v'^2}+\overline{w'^2}\right)$: (a) P01 to P12 in the near wake of the natural macrophyte; (b) $P01_T$ and $P06_T$ for the trimmed macrophyte; (c) $P01_R$ and $P06_R$ for the rough bed control; (d) P13 to P24 in the far wake of the natural macrophyte. The green dashed lines are the downstream projection of the macrophyte boundaries. The high TKE between -0.8>y>-1.0 in (a) is due to turbulence in the wake of a cobble cluster.

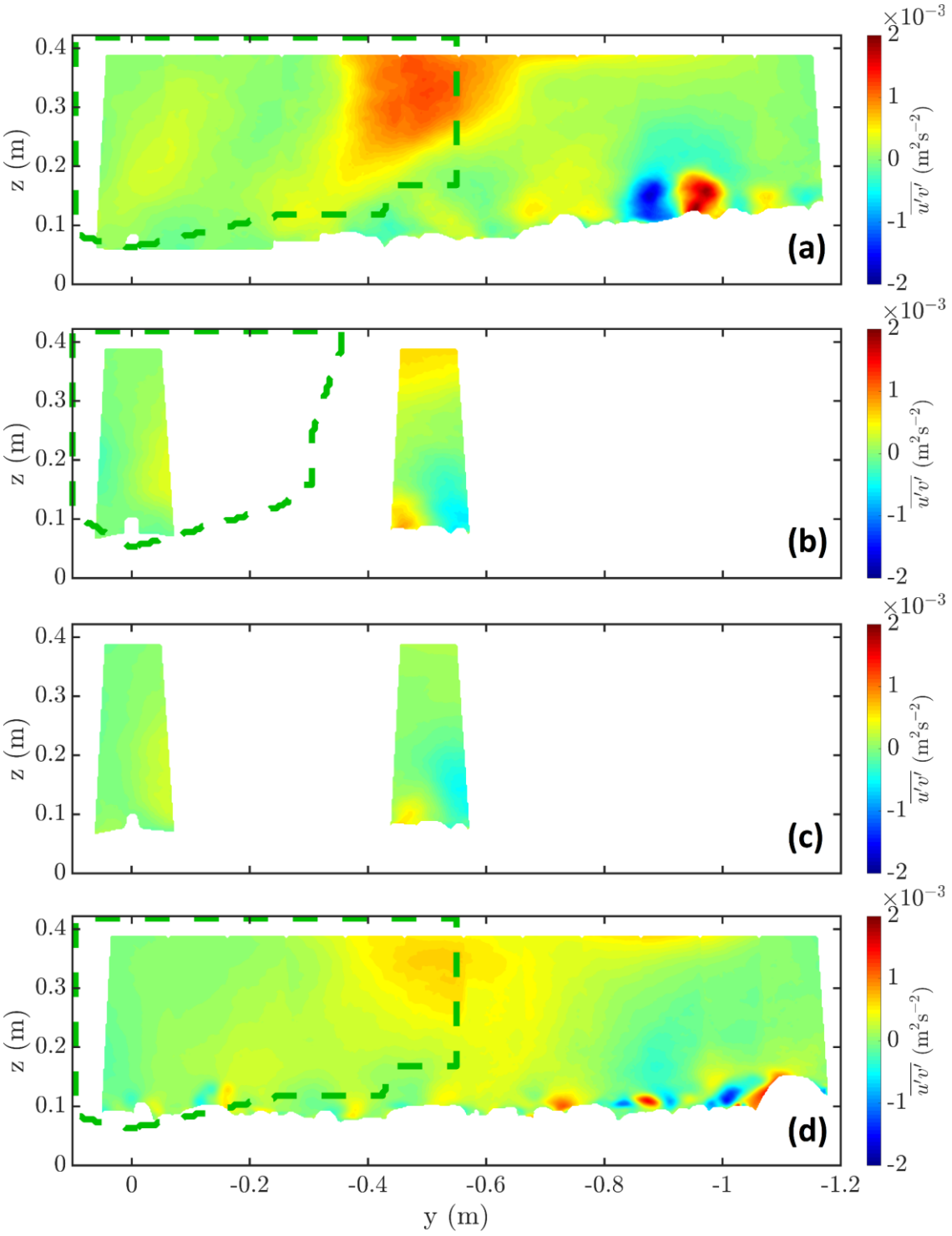

Figure 8. Velocity covariance $\overline{u'v'}$: (a) P01 to P12 in the near wake of the natural macrophyte; (b) $P01_T$ and $P06_T$ for the trimmed macrophyte; (c) $P01_R$ and $P06_R$ for the rough bed control; (d) P13 to P24 in the far wake of the natural macrophyte. The green dashed lines are the downstream projection of the macrophyte boundaries.

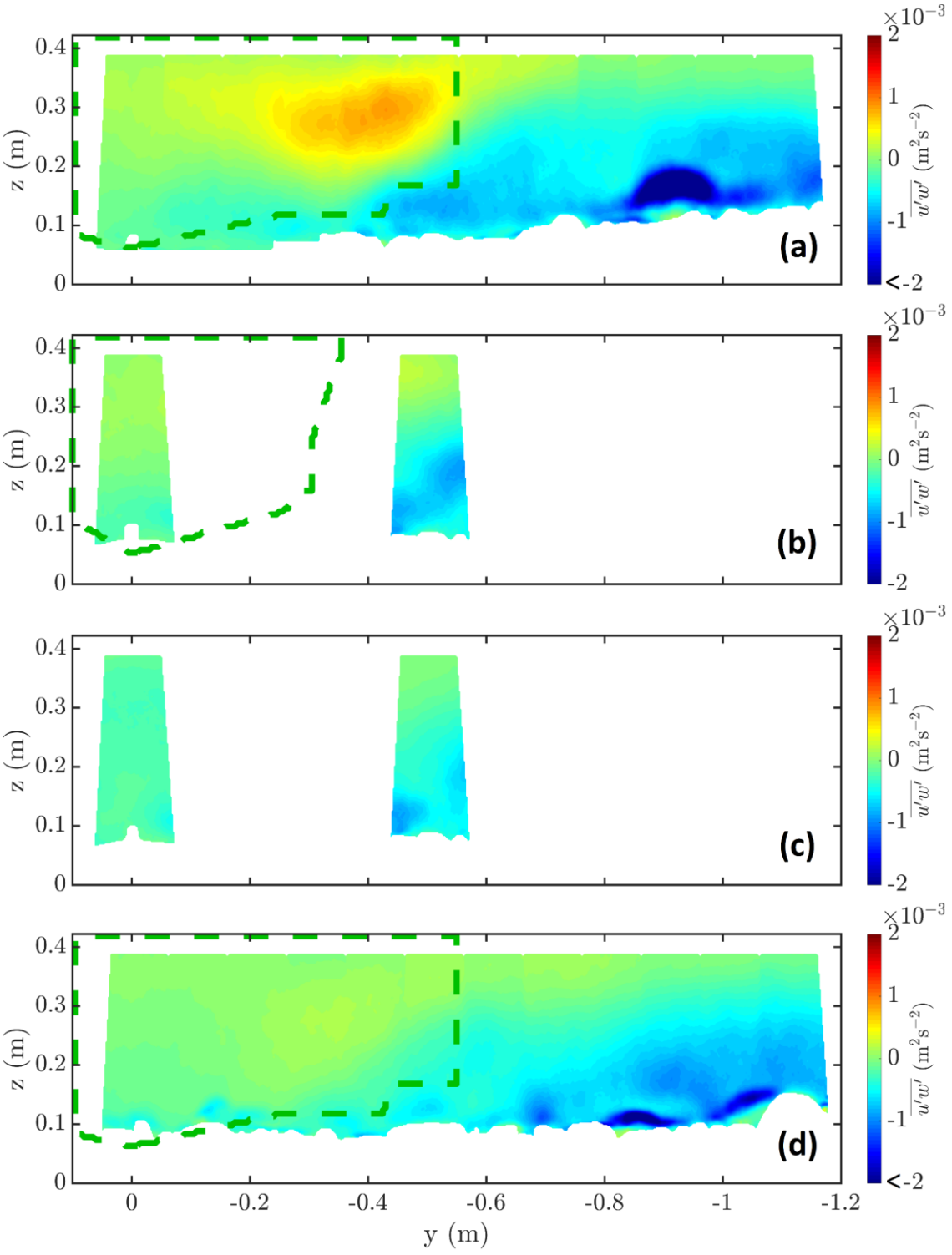

Figure 9. Velocity covariance $\overline{u'w'}$: (a) P01 to P12 in the near wake of the natural macrophyte; (b) $P01_T$ and $P06_T$ for the trimmed macrophyte; (c) $P01_R$ and $P06_R$ for the rough bed control; (d) P13 to P24 in the far wake of the natural macrophyte. The green dashed lines are the downstream projection of the macrophyte boundaries.

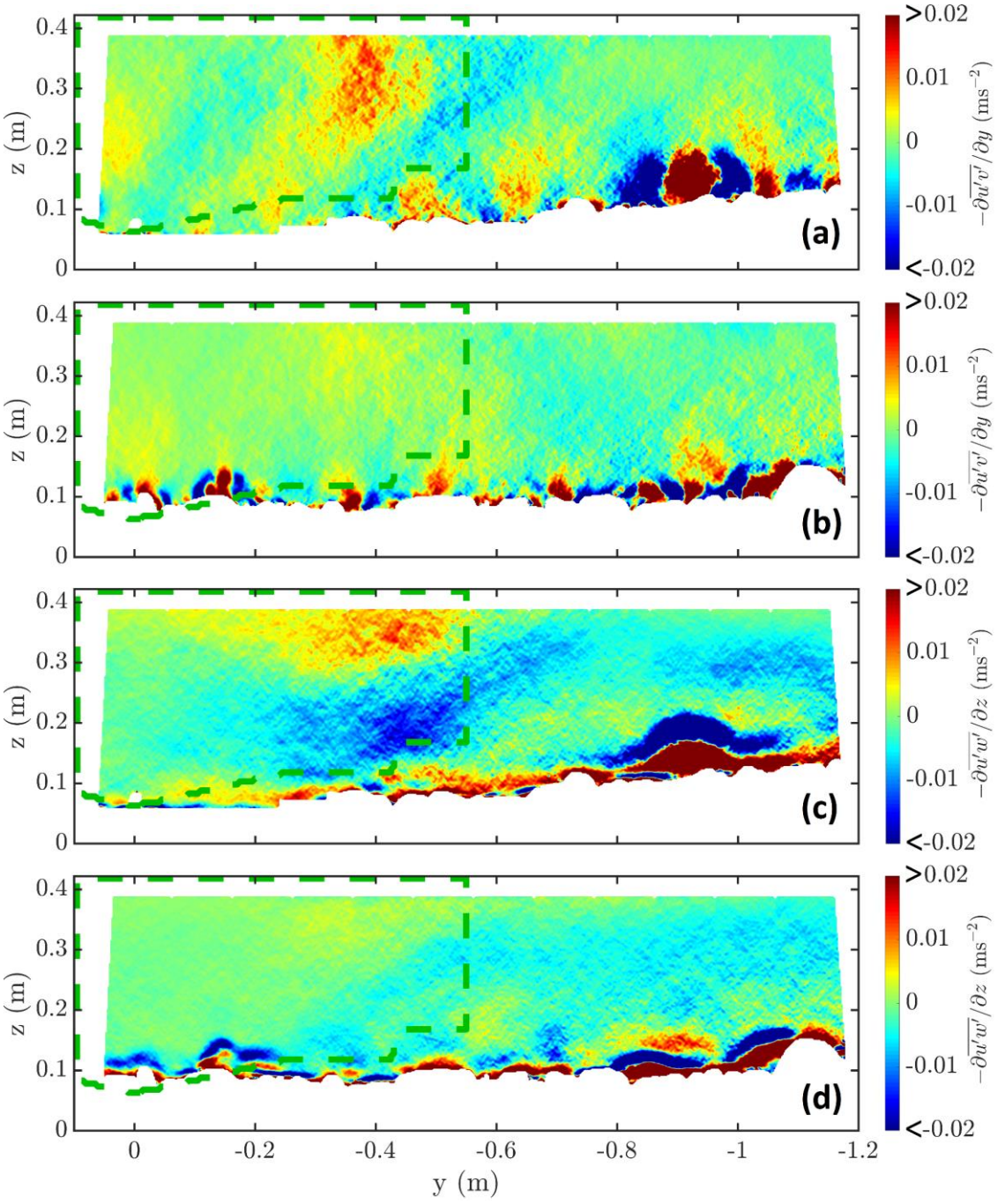

Figure 10. Streamwise mean accelerations: (a) P01 to P12 due to $-\partial\overline{u'v'}/\partial y$; (b) P13 to P24 due to $-\partial\overline{u'v'}/\partial y$; (c) P01 to P12 due to $-\partial\overline{u'w'}/\partial z$; (d) P13 to P24 due to $-\partial\overline{u'w'}/\partial z$. The green dashed lines are the downstream projection of the macrophyte boundaries. Plot limits are selected to show the downstream effect of turbulent mixing in the macrophyte wake and shear layer on streamwise mean accelerations.

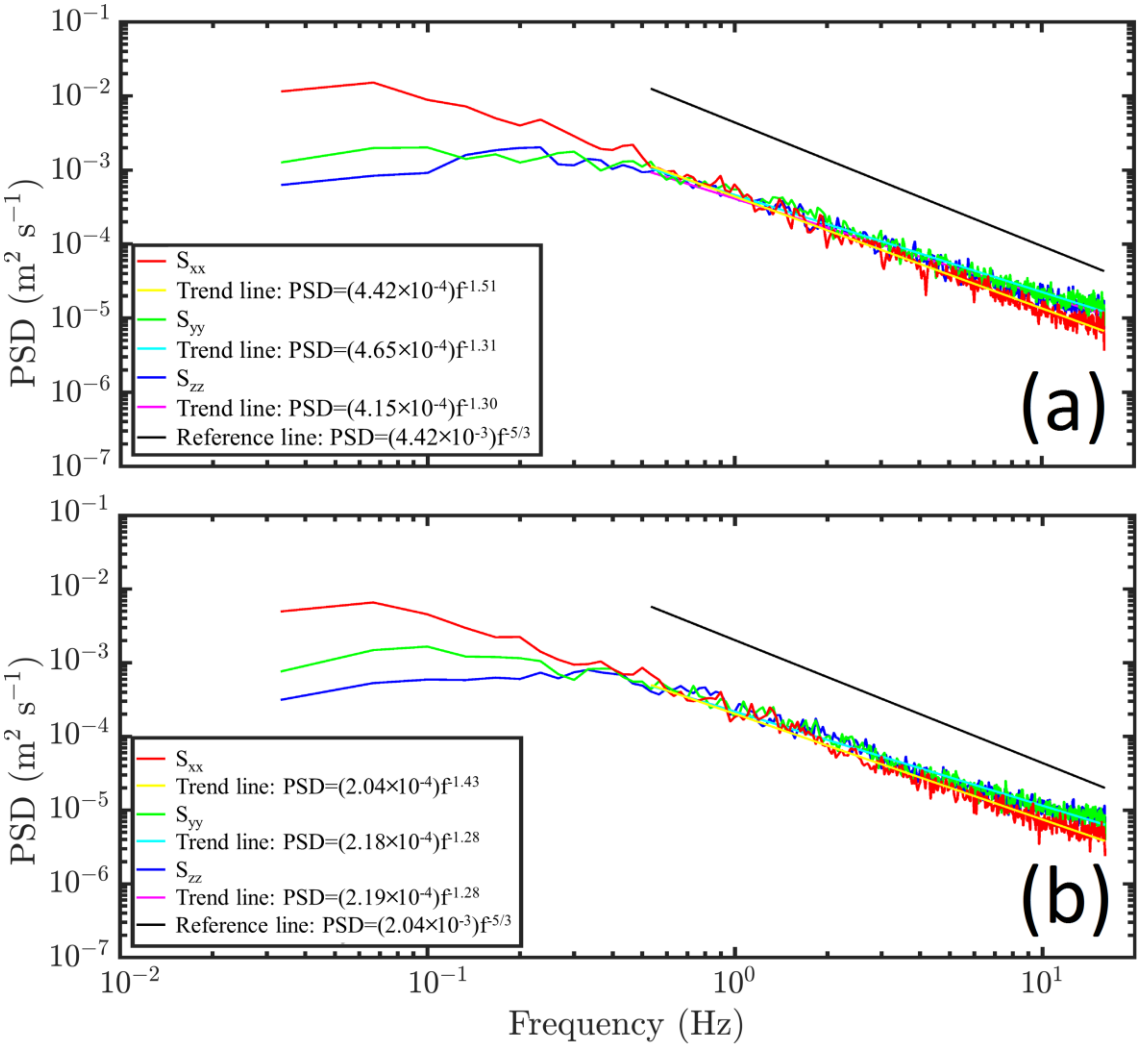

Figure 11. Power spectral density: (a) at x = 0 m, y = -0.5 m, z = 0.3 m in P06; (b) at x = 1.81 m, y = -0.5 m, z = 0.3 m in P18. Computed via Welch's periodogram approach with 30 second subsections (e.g. windows) and 50% overlap.

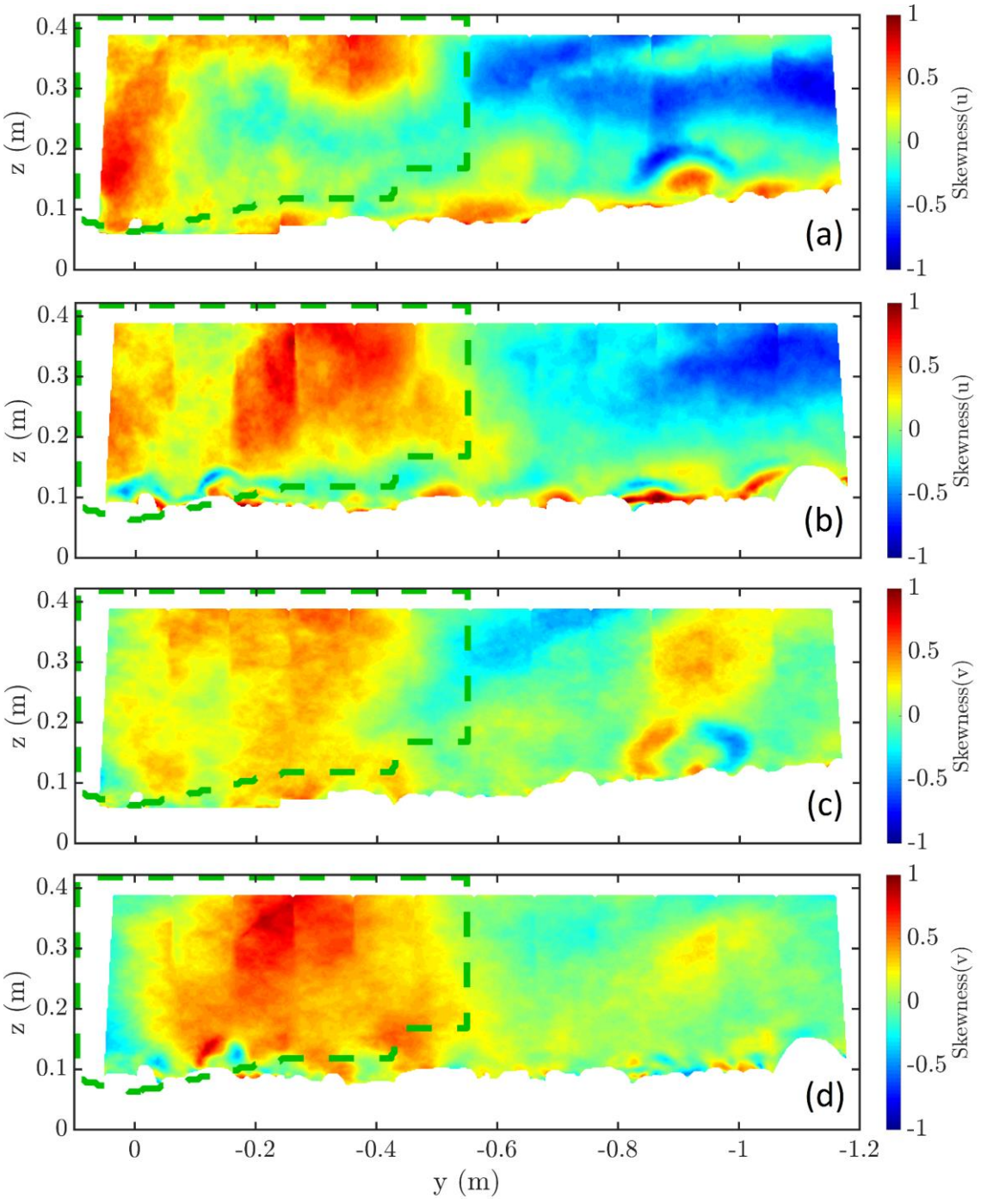

Figure 12. (a) Skewness of u for P01 to P12; (b) skewness of u for P13 to P24; (c) skewness of v for P01 to P12; (d) skewness of v for P13 to P24.

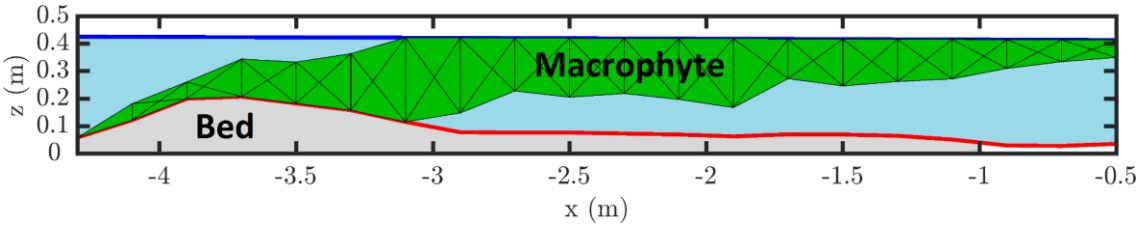

Figure 13. Substantial sedimentation occurred at the leading edge of the macrophyte, but minimal accumulation was found underneath the floating macrophyte canopy.